Two-port network compact representation of resonator arrays for wireless power transfer with variable receiver position

Received: Added at production | Revised: Added at production | Accepted: Added at production

DOI: xxx/xxxx

ARTICLE TYPE

Two-port Network Compact Representation of Resonator Arrays for Wireless Power Transfer with Variable Receiver Position

Leonardo Sandrolini[1] | Mattia Simonazzi[1] | Sami Barmada[2] | Nunzia Fontana[2]

[1]Department of Electrical, Electronic, and Information Engineering "Guglielmo Marconi" - DEI, University of Bologna, Bologna, Italy

[2]Department of Energy, Systems, Territory and Constructions Engineering (DESTEC), University of Pisa, Pisa, Italy

Correspondence
Mattia Simonazzi
Email: mattia.simonazzi2@unibo.it

Present Address
Viale del Risorgimento 2, 40136 Bologna, Italy

Summary

This paper presents an equivalent circuit characterization of an array of resonators for wireless power transfer (WPT) applications. These apparatuses are composed of magnetically coupled resonant coils acting as a transmitter which feeds a receiver coil that can be placed over them at any position, allowing the tolerance of the system to the receiver misalignment to be dramatically enhanced. This advantage makes resonator arrays a suitable solution for both low- and high-power applications. The latter usually involve battery charging, with the resonator array acting as a transformer stage, ensuring galvanic isolation. An equivalent two-port network can be defined for any receiver position, allowing the array to be treated as a traditional transformer. Thereby, the simulation of the system can be simplified, as it is required in the design steps of a converter and control strategy. Analytical expressions of the two-port network parameters are proposed for arrays of any size and length. The formulas have been numerically and experimentally validated.

KEYWORDS:
Wireless power transfer, inductive power transfer, resonator array, transformer, circuit modelling, battery charging.

1 | INTRODUCTION

In the last decade, wireless power transfer (WPT) systems have become a convenient and reliable solution in many applications, ranging from powering portable electronic devices to automatic machines and electric vehicle (EV) charging [1,2,3]. These apparatuses offer many advantages, as the ability of operating in difficult environments or the possibility to transfer power to moving loads. The size and weight of high-power batteries can be reduced by more frequent charging, which can be dramatically eased by wireless chargers. Several different technologies have been proposed in literature for both stationary and dynamic charging [4,5,6]. For high-power transfer, among near-field WPT technologies, inductive power transfer (IPT) is largely employed. One of its major limits is the misalignment between the transmitter and receiver apparatuses, which dramatically affects the efficiency and the transferred power. In order to improve the tolerance to the misalignment, arrays of magnetically coupled resonating L-C circuits (also referred as relay coils) can be used, which represent a very cheap solution since only few passive electronic components are required [7,8,9,10,11]. In these systems, the power travels from the source to the load through the relay coils at the expense of an increased sensitivity to the mismatch between the input and output side impedances [12,13], which reflects also on the magnetic near-field distribution [14]. Solutions to this problem have been proposed in [15,16], making arrays of resonators an increasingly viable option for both consumer electronics and industrial applications. Notwithstanding, a feasible implementation of relay coil assisted IPT systems requires that parameters such as voltage gain and impedance are taken into account.

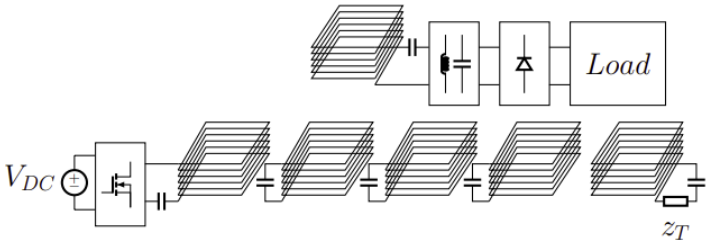

FIGURE 1 IPT system with a resonator array and a receiver over it.

In this work, as it is in high-power IPT systems, the power source feeds the array through a voltage-source inverter, whereas the load is a battery connected to the receiver by means of a rectifying stage. The IPT system behaves as an isolated power converter where the resonator array and the receiver act as the transformer stage [17,18]. In modern isolated power converters, the high-power rate required by the load makes the soft-switching operation of the input inverter necessary [19,20,21] and the design of power electronics components and control strategy requires an adequate model of the system. When considering arrays of magnetically coupled resonators different equivalent models can be defined and have been proposed [22,23,24], although they usually apply to simple network topologies. This paper aims to define a general and accurate model of the system valid for any receiver position and load condition. In particular, a two-port network has been chosen to represent the resonator array coupled to a receiver coil when employed as transformer stage in IPT apparatuses, with the purpose of evaluating its performance. The analytical expressions of the transmission matrix parameters of the two-port network are derived and validated both numerically and experimentally. The results obtained with the proposed approach are discussed with reference to the theory of resonator arrays [12,25,26].

The manuscript is organized as follows: in Sec. 2 the array of resonators is described and its impedance matrix is defined; in Sec. 3 the methodology for the extraction of the equivalent circuit parameters is proposed. In Sec. 4 the results of numerical simulations are reported and discussed. In Sec. 5, the resonator array is described with the equivalent circuit of a loaded transformer and finally in Sec. 6 the results of experimental measurements performed on a prototype are presented and compared with the analytically calculated values.

2 | RESONATOR ARRAY FOR INDUCTIVE POWER TRANSFER

The inductive coupling system presented in this paper consists of a primary side realized with an array of n magnetically coupled coils arranged along a line, which transmits power to a receiver coil placed over it, as depicted in Fig. 1. All the array coils are identical and equally spaced, so that the mutual inductance M is the same for each couple of adjacent cells. According to [12,25], the mutual inductance between non adjacent coils can be neglected and the so called “nearest-neighborhood approximation" holds. The receiver is free to be placed over any cell of the array and then the mutual inductance $M_{r,i}$ between the receiver and the ith facing cell is the same for each position, being all the cells identical. Each coil is characterized by an intrinsic resistance R and resonates with a series lumped capacitor at the resonant frequency $f_0 = 1/(2\pi\sqrt{LC})$, where L is the intrinsic self-inductance of each resonator and C the lumped capacitance. The lumped-circuit parameters can be determined with analytical formulas taken from the literature, as shown in [27]. In this work, a general equivalent load z_{load} is considered, which is assumed connected to the receiver circuit. In case of battery charging applications, the array is fed by a voltage source inverter, whereas the receiver is connected to a typical battery charger load, composed of a matching network, a rectifying and filtering stage, a DC/DC converter and the battery. A further degree of freedom is obtained with the addition in the last cell of the array of a termination load z_T, which can be adjusted to maximize the transfer efficiency, as described in [15]. In order to optimize the efficiency, the modulation of the termination impedance proposed in [16] can be implemented, making it possible to assume similar operating conditions for each position of the receiver. The analysis can be carried out considering the fundamental components of current and voltage, which can be treated as phasors at the resonant angular frequency $\omega_0 = 2\pi f_0$. The circuit model of the overall system has been derived and discussed in [28], with the characterization of the half-bridge inverter feeding the apparatus and the load. For the aim of this paper, the equivalent circuit of the array depicted in Fig. 2 is considered.

It must be noticed that, in case of dynamic charging, the receiver moves over the array and the mutual inductance $M_{r,i}$ is subject to vary according to the receiver position [25]. However, for a sufficiently high operating frequency, the motional electromotive

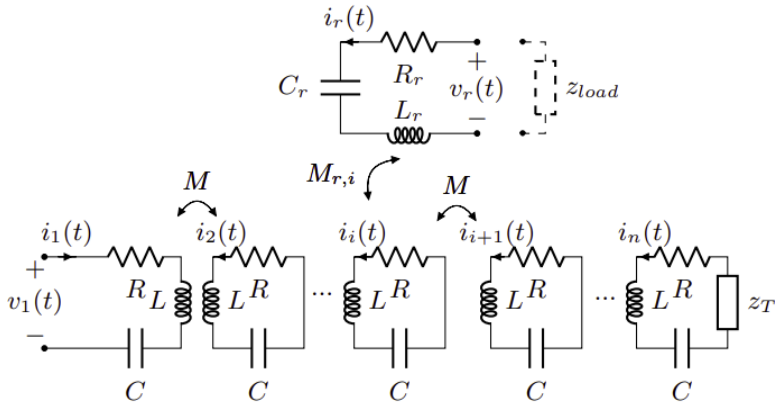

FIGURE 2 Equivalent circuit of an IPT system composed of a resonator array and a receiver.

force (emf) due to the receiver movement can be considered negligible with respect to the transformer emf, as discussed in [26]. Consequently, dynamic charging can then be studied with the same methodology applied to static charging. During the movement the receiver can be coupled to two array resonators at a time; however, being the prominent positions those corresponding to a perfect alignment of the receiver with the array resonators [25], the following analysis considers aligned positions of the receiver.

3 | TWO-PORT REPRESENTATION

In order to obtain a compact representation of the array of resonators, the impedance matrix is adopted, but other configurations can be derived from that, depending on the needs of the designer [23]. The inductive coupling is characterized as a unique two-port network, considering the terminals of the first resonator as the input port and the ones of the receiver as the output port, where $\hat{V}_1$, $\hat{I}_1$ and $\hat{V}_r$, $\hat{I}_r$ are the phasors associated to the voltages and currents $v_1(t)$, $i_1(t)$ and $v_r(t)$, $i_r(t)$, respectively. The currents circulating in the resonators are very sensitive to the variations of the array parameters, which in turn affect the transmission capability of the system. In general, for a fixed load, termination and input voltage, all the currents and voltages involved in the circuits present different values depending on the receiver position, thereby complicating the design of the control system with respect to the traditional isolated power converters. Thus, a different matrix should be written for any receiver position. In sinusoidal steady-state, considering the equivalent circuit depicted in Fig. 2, it is possible to define the impedance matrix of the equivalent two-port network from the following system of equations:

$$\begin{bmatrix} \hat{V}_1 \\ \hat{V}_r \end{bmatrix} = \begin{bmatrix} \hat{Z}_{11} & \hat{Z}_{1r} \\ \hat{Z}_{r1} & \hat{Z}_{rr} \end{bmatrix} \begin{bmatrix} \hat{I}_1 \\ \hat{I}_r \end{bmatrix} \tag{1}$$

where

$$\begin{aligned} \hat{Z}_{11} &= \left.\frac{\hat{V}_1}{\hat{I}_1}\right|_{\hat{I}_r=0} \quad \hat{Z}_{1r} = \left.\frac{\hat{V}_1}{\hat{I}_r}\right|_{\hat{I}_1=0} \\ \hat{Z}_{r1} &= \left.\frac{\hat{V}_r}{\hat{I}_1}\right|_{\hat{I}_r=0} \quad \hat{Z}_{rr} = \left.\frac{\hat{V}_r}{\hat{I}_r}\right|_{\hat{I}_1=0}. \end{aligned} \tag{2}$$

3.1 | Extraction of the Impedance-Matrix Parameters

The analytical expressions of the impedance-matrix parameters are derived for an array of n resonators with a receiver coupled with the ith cell only (see Fig. 3 a). As first step, the resonators that follow the one covered by the receiver - namely from the $(i+1)$th to the nth one - have been substituted with their equivalent impedance seen from the ith cell. According to [29], the

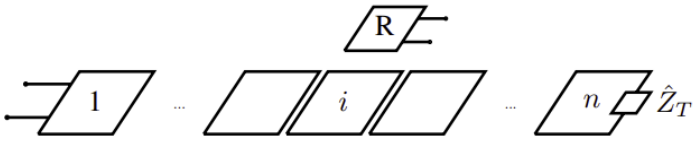

a)

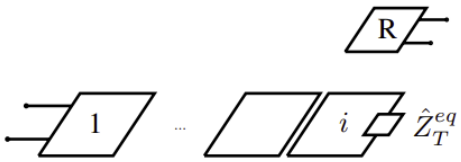

b)

FIGURE 3 Schematic representation of (a) an array of n resonators with a receiver R over the ith cell, terminated with $\hat{Z}_T$ and (b) the correspondent compacted array terminated with the equivalent impedance (4).

equivalent impedance of an array of m resonators terminated with an impedance $\hat{Z}_{end}$ is defined as:

$$\hat{Z}^{eq}_{m,\hat{Z}_{end}} = \cfrac{(\omega M)^2}{\hat{Z}+\cfrac{(\omega M)^2}{\ldots+\cfrac{(\omega M)^2}{\hat{Z}+\cfrac{(\omega M)^2}{\hat{Z}+\hat{Z}_{end}}}}} \tag{3}$$

where $\hat{Z} = R+j\omega L+1/(j\omega C)$ is the impedance of each resonator. Then, for the considered case, $m = n-i$ and $\hat{Z}_{end} = \hat{Z}_T$.

The resulting compacted array is schematically represented in Fig. 3 b): it is composed of the remaining i resonators and terminated with the impedance

$$\hat{Z}^{eq}_T = \hat{Z}^{eq}_{n-i,\hat{Z}_T}\ , \tag{4}$$

whereas the receiver is placed over the last cell. Writing a Kirchhoff voltage equation for each resonator of the compacted array, the following system of $i+1$ equations holds:

$$\begin{aligned}
\hat{V}_1 &= \hat{Z}\hat{I}_1+j\omega M\hat{I}_2\\
0 &= \hat{Z}\hat{I}_2+j\omega M\hat{I}_1+j\omega M\hat{I}_3\\
&\vdots\\
0 &= \hat{Z}\hat{I}_{i-1}+j\omega M\hat{I}_{i-2}+j\omega M\hat{I}_i\\
0 &= (\hat{Z}+\hat{Z}^{eq}_T)\hat{I}_i+j\omega M\hat{I}_{i-1}+j\omega M_{r,i}\hat{I}_r\\
\hat{V}_r &= \hat{Z}_r\hat{I}_r+j\omega M_{i,r}\hat{I}_i
\end{aligned} \tag{5}$$

which can be reduced - by removing the equations of all the resonators but the first one and the receiver - to the system:

$$\begin{aligned}
\hat{V}_1 &= \hat{Z}_{11}\hat{I}_1+\hat{Z}_{1r}\hat{I}_r\\
\hat{V}_r &= \hat{Z}_{rr}\hat{I}_r+\hat{Z}_{r1}\hat{I}_1.
\end{aligned} \tag{6}$$

The parameters that result from this mathematical manipulation correspond to the ones of the impedance matrix (2), whose analytical expressions are:

$$\hat{Z}_{11} = \hat{Z}+\hat{Z}^{eq}_{n-1,\hat{Z}^{eq}_T} \tag{7}$$

$$\hat{Z}_{rr} = \hat{Z}_r+\frac{(\omega M_{r,i})^2}{\hat{Z}+\hat{Z}^{eq}_T+\hat{Z}^{eq}_{i-2,0}} \tag{8}$$

$$\hat{Z}_{1r} = \hat{Z}_{r1} = \frac{M_{r,i}}{M}\left(\frac{1}{(j\omega M)^{i-2}}\prod_{k=1}^{i-1}\hat{Z}^{eq}_{k,\hat{Z}^{eq}_{T}}\right). \tag{9}$$

These formulas are valid for arrays of the type described in Sec. 2, with any number of resonators, termination impedance and considering the receiver aligned with any cell of the array. Moreover, introducing the expressions presented in[30] in (7)-(9), it is possible to obtain a closed-form formulation of the two-port network parameters.

4 | NUMERICAL SIMULATIONS AND RESULTS

The analytical expressions of the impedance-matrix parameters can be validated comparing the results they provide with the ones obtained through a numerical simulation of the WPT system. In this work, the validation is achieved solving the Kirchhoff voltage equations written for each cell of the system, considering phasors at f_0. The equations can be arranged in matrix form as:

$$\hat{\mathbf{V}} = \hat{\mathbf{Z}}_i\hat{\mathbf{I}} \tag{10}$$

where $\hat{\mathbf{I}}$ is the vector of the phasor currents flowing in the resonators and $\hat{\mathbf{V}} = [\hat{V}_1 0 ... 0 \hat{V}_r]^T$ is the phasor voltage vector with $\hat{V}_1$ the phasor supply voltage of the transmitter, and $\hat{V}_r$ the phasor voltage at the output terminals. $\hat{\mathbf{Z}}_i$ is the $(n+1)\times(n+1)$ impedance matrix of the resonator array which, for a generic receiver position, can be written as:

$$\hat{\mathbf{Z}}_i = \begin{bmatrix} \hat{Z} & j\omega M & 0 & 0 & \cdots & 0 \\ j\omega M & \hat{Z} & j\omega M & 0 & \cdots & 0 \\ 0 & \vdots & \ddots & \vdots & \cdots & j\omega M_{i,r} \\ \vdots & \vdots & \vdots & \ddots & \vdots & \vdots \\ \vdots & 0 & \cdots & j\omega M & \hat{Z}+\hat{Z}_T & 0 \\ 0 & 0 & j\omega M_{r,i} & 0 & \cdots & \hat{Z}_r \end{bmatrix} \tag{11}$$

where the last row considers the coupling of the receiver with the *i*th resonator of the array . As the receiver moves, the impedance matrix modifies according to its position, thereby leading to a different system of equations to be solved.

The impedance-matrix terms (1) are numerically derived solving the system of equation described in (10) when the input and output ports of the apparatus are properly terminated in open circuit, as described in (2). By connecting the input port to an impedance $\hat{Z}_S$, $\hat{V}_1 = -\hat{Z}_S\hat{I}_1$ and (10) can be rearranged and solved for $\hat{\mathbf{I}}$ for an arbitrary value of $\hat{V}_r$. Enforcing $\hat{Z}_S$ to a value large enough to have $\hat{I}_1 \approx 0$, we can determine $\hat{Z}_{rr}$ and $\hat{Z}_{1r}$ from $\hat{V}_r$, $\hat{I}_r$ and

$$\hat{V}_1\Big|_{\hat{I}_1=0} = \hat{Z}_{i(1,2)}\hat{I}_2 \ , \tag{12}$$

with $\hat{Z}_{i(1,2)}$ the element of the first row and second column of (11).

Analogously, for the calculation of $\hat{Z}_{11}$ and $\hat{Z}_{r1}$, an impedance $\hat{Z}_{load}$ is connected to the output port so that $\hat{V}_r = -\hat{Z}_{load}\hat{I}_r$. Thus, rearranging and solving (10) for $\hat{\mathbf{I}}$ for an arbitrary value of $\hat{V}_1$, we can determine $\hat{I}_1$ and, in turn, $\hat{Z}_{11}$ by enforcing $\hat{Z}_{load}$ to a value large enough to have $\hat{I}_r \approx 0$. The impedance $\hat{Z}_{r1} = \hat{Z}_{1r}$ due to the reciprocity of the network and can be determined from $\hat{I}_1$ and

$$\hat{V}_r\Big|_{\hat{I}_r=0} = \hat{Z}_{i(r,i)}\hat{I}_i \ , \tag{13}$$

where $\hat{Z}_{i(r,i)} = j\omega M_{r,i}$ is the element of the last row and last but one column of (11) and $\hat{I}_i$ the current of the *i*th resonator.

4.1 | Validation results

For the numerical simulations, the prototype of resonators employed in the experimental setup are considered.

Each resonator of the array is realized with a 6-turn square winding of 153 mm side-length. The stranded wire conductors have a section of 2.5 mm^2, that results in an intrinsic resistance $R = 0.05\,\Omega$ and a self-inductance $L = 11.9\,\mu$H. The mutual inductance between the adjacent resonators is $M = -1.67\,\mu$H. The lumped capacitors connected to the coils present a capacitance of $1\,\mu$F, making the system resonate at $f_0 = 45.1$ kHz. The receiver winding is realized with 5-turns of copper wire wound around a circular plastic core with a diameter of 9 cm, resulting in a resistance $R_r = 0.055\,\Omega$ and a self-inductance $L_r = 3.8\,\mu$H, whereas the mutual inductance between the receiver and the facing resonator of the array is 1.13 μH. It is connected to a lumped capacitance C_r of $3.3\,\mu$F. The simulations are carried out for the cases of short-circuit (SC) and matched terminations of the array. The termination impedance can be calculated as $Z_0 \approx \omega_0 M$ [7,29] and its value is about 0.47 Ω for the considered system.

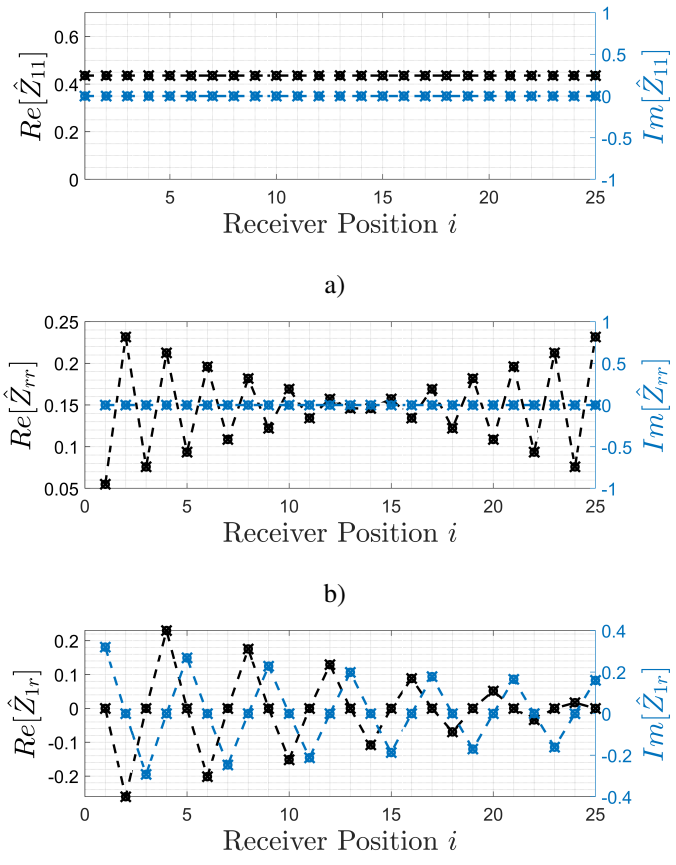

FIGURE 4 Z-matrix parameters as a function of the receiver position for an array of 25 resonators at the resonant frequency f_0 in case of short-circuit termination. The cross and circle markers refer to the formulas (7)-(9) and numerical solution of (10), respectively

The impedance-matrix parameters of an array of 25 resonators are plotted with the receiver aligned with each resonator, in case of short-circuit and matched termination in Figs. 4 and 5, respectively. In particular, the plots compare the trends obtained with the formulas (7)-(9) and the numerical solution of (10), showing that they are in perfect agreement being the curves overlapped. The reported values are calculated considering the system operating at f_0. As it is possible to observe, the parameters $\hat{Z}_{11}$, $\hat{Z}_{rr}$ and $\hat{Z}_{1r}$ behave very differently: while both the real and imaginary parts of $\hat{Z}_{11}$ remain almost constant, $\hat{Z}_{rr}$ and $\hat{Z}_{1r}$ strongly vary depending on the receiver position.

$\hat{Z}_{11}$

The trend of $\hat{Z}_{11}$ in Figs. 4 a) and 5 a) can be explained considering its definition, reported in (7). Indeed, it is calculated considering the output port open, meaning that the receiver does not interact with the array. The impedance seen from the array input port is purely real and remains the same for any receiver position, whereas it is affected by the number of resonators and the termination $\hat{Z}_T$ only. A detailed analysis is provided in[29].

$\hat{Z}_{rr}$

For what concerns $\hat{Z}_{rr}$, it is characterized by a null imaginary part, whereas the real part oscillates according to the receiver position around 0.16 Ω in case of short-circuit termination 0.15 Ω in case of matched termination, shown in Figs. 4 b) and 5 b), respectively). In particular, for $\hat{Z}_T = 0$, Re$[\hat{Z}_{rr}]$ oscillates with decreasing amplitude until the receiver covers the cells in the first half of the array ($i < n/2$), whereas the trend is inverted for $i > n/2$.

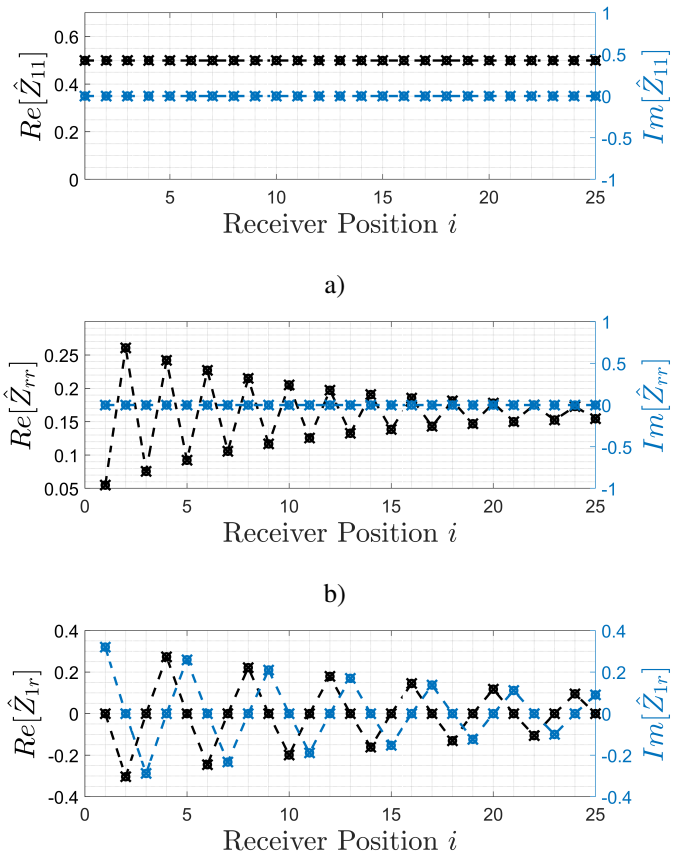

FIGURE 5 Z-matrix parameters as a function of the receiver position for an array of 25 resonators at the resonant frequency f_0 in case of matched termination. The cross and circle markers refer to the formulas (7)-(9) and numerical solution of (10), respectively

This can be explained as, for a short-circuited array, both $\hat{Z}_T^{eq}$ and $\hat{Z}_{i-2,0}^{eq}$ oscillates according to[29], leading to the trend depicted in Fig. 4 b). As the receiver approaches the central array resonator, the $\hat{Z}_T^{eq}$ and $\hat{Z}_{i-2,0}^{eq}$ tends to the same value, but with opposite periodicity, until they cancel for $i = (n\pm1)/2$. Differently, in case of a matched array, Fig. 5 b), $\hat{Z}_T^{eq}$ is always equal to the matching impedance and, assuming $M_{r,i}$ constant, the only varying term of (8) is $\hat{Z}_{i-2,0}^{eq}$, which behaves as the input impedance of a short-circuited array, as it is well described in[29].

$\hat{Z}_{1r}$

The term $\hat{Z}_{1r} = \hat{Z}_{r1}$ has a similar behaviour for both the considered terminations. It presents a real and an imaginary part alternatively null, which both oscillate around zero and whose amplitudes decrease as the receiver moves away from the input port. The attenuation of Re$[\hat{Z}_{1r}]$ is due to Joule losses in the resonator windings and it is more evident if $\hat{Z}_T = 0$. The peculiarity of the results lies in the purely real values that $\hat{Z}_{1r}$ assumes when the receiver is aligned with even numbered resonators (regardless of n being even or odd) and that can be also negative. Indeed, this parameter expresses the link between the input and output ports of the network and, for magnetically coupled resonators, it is usually associated to the overall mutual inductance between the resonators connected to the ports. The currents circulating in adjacent resonators are $\pi/2$ out of phase and thus the trends of Re$[\hat{Z}_{1r}]$ and Im$[\hat{Z}_{1r}]$ reflect this peculiarity.

5 | TRANSFORMER EQUIVALENT CIRCUIT

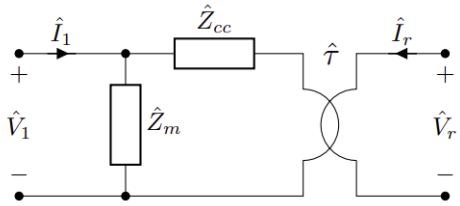

FIGURE 6 Equivalent circuit of a loaded real transformer.

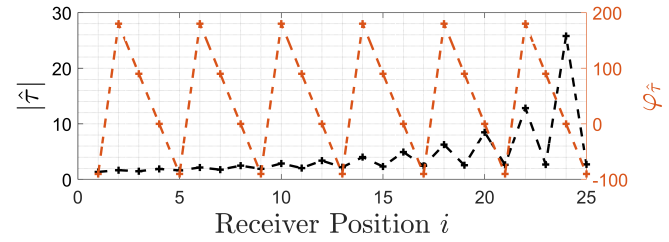

a)

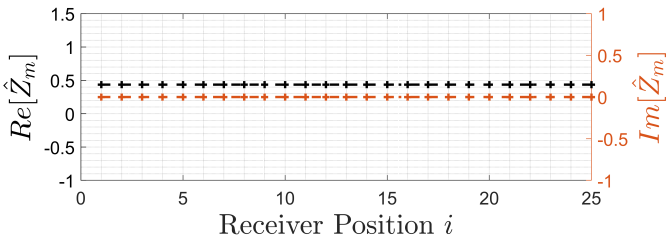

b)

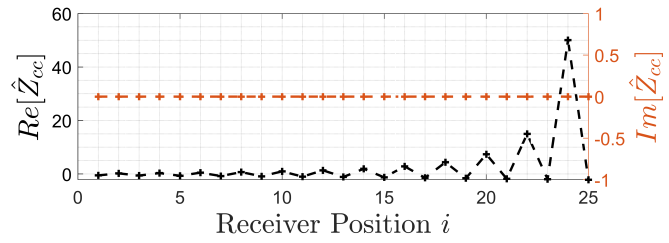

c)

FIGURE 7 Parameters of the real transformer equivalent circuit as a function of the receiver position for an array of 25 resonators at the resonant frequency f_0 in case of short-circuit termination.

IPT systems behave as isolated power converters where the transformer stage is composed of the transmitter and the receiver. In particular, battery chargers must provide the appropriate battery voltage profile, whereas minimizing the losses at the same time. Thus, the impedance parameters and the voltage gain are necessary for designing both the system and the control strategy.

For the design of isolated power converters, the most common circuit model adopted to represent loaded transformers is the one reported in Fig. 6, which allows a physical interpretation of the parameters involved. Indeed, in typical real transformers, the longitudinal parameter represents the series of the winding resistance and leakage inductance of the two windings, whereas the transverse one is associated to the magnetizing reactance. The model is completely described by three complex parameters, namely the magnetizing impedance $\hat{Z}_m$, the short-circuit impedance $\hat{Z}_{cc}$ and the transformer ratio $\hat{\tau}$. Thus, the impedance matrix

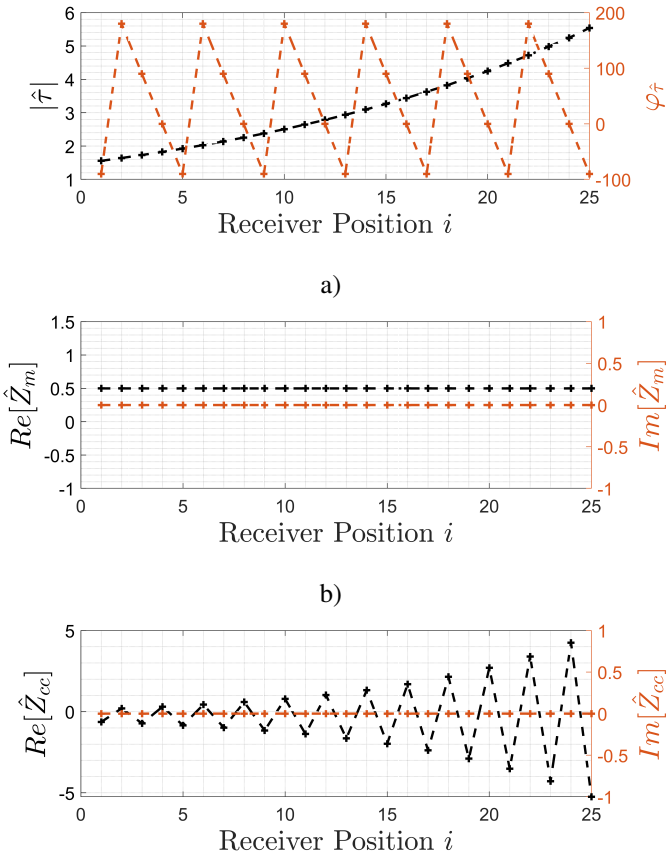

FIGURE 8 Parameters of the real transformer equivalent circuit as a function of the receiver position for an array of 25 resonators at the resonant frequency f_0 in case of matched termination.

associated to this two-port network can be written as:

$$\begin{bmatrix} \hat{V}_1 \\ \hat{V}_r \end{bmatrix} = \begin{bmatrix} \hat{Z}_m & \frac{\hat{Z}_m}{\hat{\tau}} \\ \frac{\hat{Z}_m}{\hat{\tau}} & \frac{\hat{Z}_{cc}+\hat{Z}_m}{\hat{\tau}^2} \end{bmatrix} \begin{bmatrix} \hat{I}_1 \\ \hat{I}_r \end{bmatrix}. \tag{14}$$

By means of this equivalent circuit, a resonator array coupled with a receiver can be formally represented as a real transformer. Through the application of the procedure proposed in Sec. 3.1, the parameters of the real transformer equivalent circuit can be found equating the terms of the impedance matrices in (1) and (14):

$$\begin{aligned} \hat{\tau} &= \frac{\hat{Z}_{11}}{\hat{Z}_{1r}} \\ \hat{Z}_m &= \hat{Z}_{11} \\ \hat{Z}_{cc} &= \hat{\tau}^2 \hat{Z}_{rr} - \hat{Z}_{11} \end{aligned} \tag{15}$$

and plotted as a function of the receiver position for different array terminations in Figs. 7 and 8. These plots highlight a clear dependency of the parameters on both the receiver position and array termination, as it is for the impedance matrix terms depicted in Figs. 4 and 5. In particular, the transformer ratio $\hat{\tau}$ is complex and its amplitude increases as the receiver is moved away from the power source with an oscillatory behaviour in case of SC termination and a nearly linear trend in case of matching termination. Barring losses, this parameter indicates the ratio between the input and output voltages $\hat{V}_1$ and $\hat{V}_r$ of the two-port network and shows that, for a fixed $\hat{V}_1$, $\hat{V}_2$ decreases as the receiver moves away from the power source. Its value is very sensitive to the receiver position in case of SC termination, whereas its magnitude has a smoother trend matching the termination of the array. The phase of $\hat{\tau}$ presents a periodic behaviour for both terminations and indicates the phase variation that the

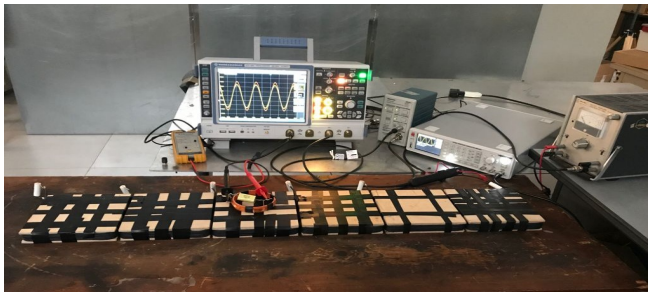

FIGURE 9 Experimental Setup.

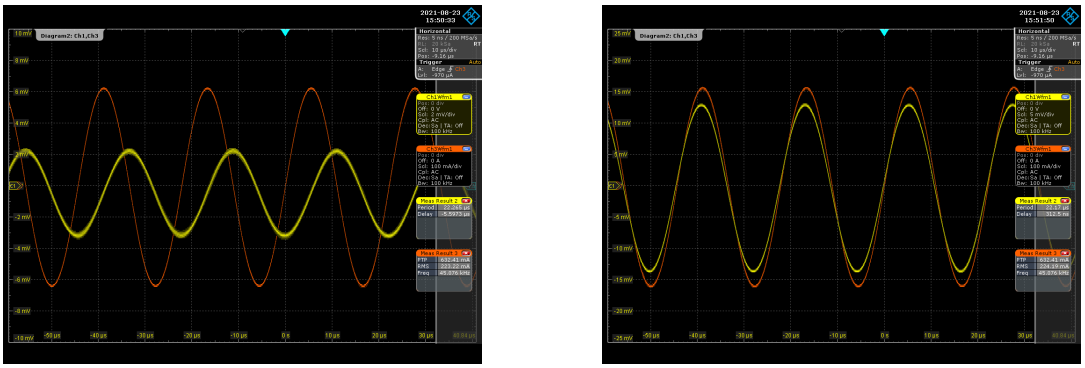

(a) **(b)**

FIGURE 10 The orange waveform represents the current in the first array resonator and the yellow one the voltage across the receiver port, when the receiver is on a) the 3rd and b) the 4th array cell.

receiver voltage undergoes in relation to the number of resonators of the array that are placed in between the receiver and the power source. The magnetizing reactance $\hat{Z}_m$ corresponds to $\hat{Z}_{11}$, which is purely real and constant for any receiver position. In traditional transformers, it presents a very large value, making it negligible during full-load operations; conversely, for the resonator array considered, its value is small and thus the current flowing through it is not always negligible with respect to that flowing through $\hat{Z}_{cc}$, especially when the receiver is close to the power source. For what concerns $\hat{Z}_{cc}$, it results purely real for any receiver position and array termination, with a trend that oscillates between negative and positive values (the latter being the largest) for both the terminations considered. In particular, the minimum values are found when the receiver is aligned with the odd-numbered cells of the array.

6 | EXPERIMENTAL VALIDATION

The analytical and numerical procedures for the extraction of the impedance matrix parameters have been experimentally validated with a prototype of resonator array. The system is depicted in Fig. 9 and it is described in 4.1. Current and voltage measurements have been performed at the system input and output ports and the impedance matrix parameters have been estimated according to (2). In particular, the supplied port has been fed with a sinusoidal voltage at the system-resonant frequency generated by a Hameg signal generator and amplified by an analog amplifier. The current measurements have been performed with a current probe Tektronix TCP305A amplified by a Tektronix “TCPA 300" connected to a Rohde&Schwarz RTO 1004 oscilloscope with a sampling capability of 10 GSa/s and bandwidth of 600 MHz. The voltage was measured with an isolated Pico probe “TA057" with a bandwidth of 25 MHz. As an example, in Figs. 10 a) and b) the current and voltage waveforms considered for the estimation of $\hat{Z}_{r1}$ are shown for a receiver aligned with the 3rd and 4th array cell, respectively. In the former case, the input current (orange waveform) lags the receiver voltage (yellow curve) by $\frac{\pi}{2}$, whereas in the latter the two waveforms are in phase, as predicted in Sec. 4.1.

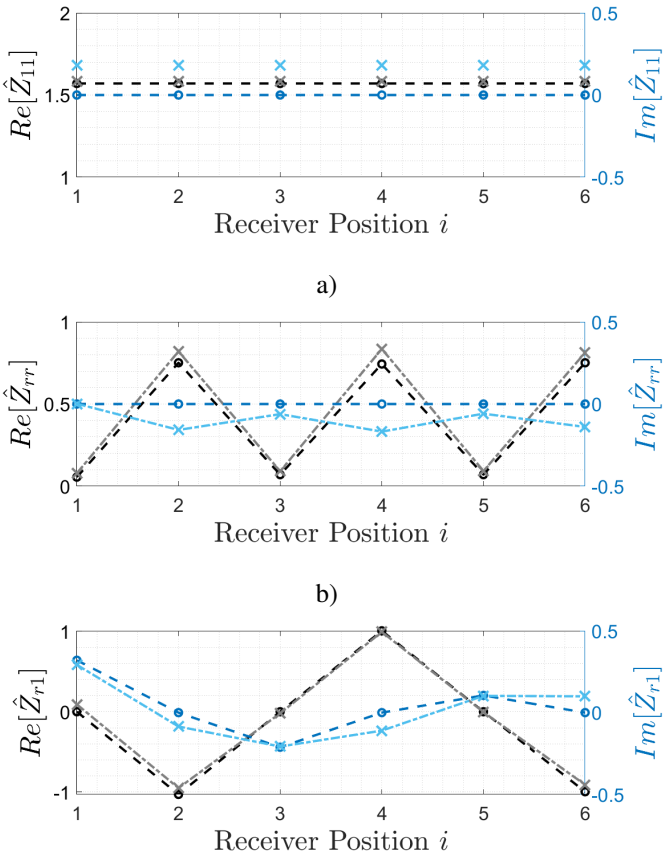

FIGURE 11 Z-matrix parameters as a function of the receiver position for an array of 6 resonators at the resonant frequency of 45.1kHz in case of short-circuit termination. The circle and cross markers refer to the formulas (7)-(9) and experimental results, respectively.

The results of the measurements are shown in Figs. 11 and 12 for the cases of short-circuit and matched terminations of the array, respectively, and are compared with the values obtained with the analytical formulas (7), (8) and (9). The plots show a very good agreement between the analytical and experimental results, even though a slightly larger difference can be observed for both the real and imaginary parts of $\hat{Z}_{rr}$ for both the considered terminations. This difference can be attributable to the mutual coupling between the receiver and the array resonators next to it. In the theoretical model, only the mutual inductance between the receiver and the resonator below it is considered, as it is generally much larger than the mutual inductance between the receiver and the other array resonators. It should be noticed that the parameters $\hat{Z}_{11}$ and $\hat{Z}_{r1}$ have been estimated feeding the first resonator of the array and measuring the voltage at the terminals of the same resonator and receiver, respectively Thus, for both measurements, the receiver operates in no-load conditions and experiences a null current, meaning that it does not interact with the array. Instead, the current and voltage considered for the estimation of $\hat{Z}_{rr}$ have been measured directly at the port of the receiver, which slightly couples with the cells of the array close to it. This effect is more evident when the receiver is above even numbered resonators, for which positions the equivalent impedance of the system seen by the receiver presents higher values and the circulating current lower magnitudes.

7 | CONCLUSIONS

In this paper, a two-port network is chosen to represent the array of resonators in a compact way, well appropriate for evaluating its performance when employed as a transformer stage in an IPT apparatus. It should be noticed that, representing the array

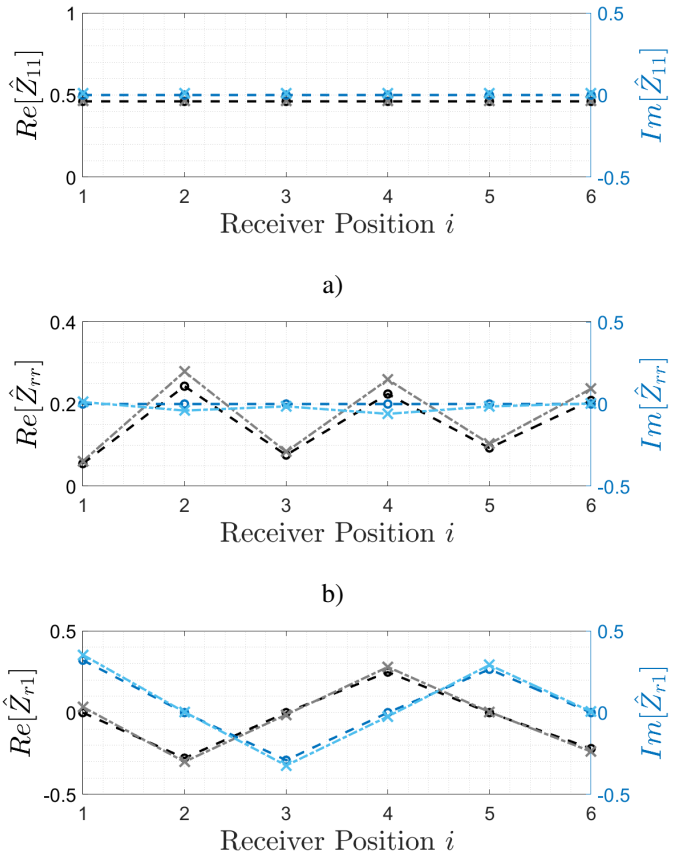

FIGURE 12 Z-matrix parameters as a function of the receiver position for an array of 6 resonators at the resonant frequency of 45.1kHz in case of matched termination. The circle and cross markers refer to the formulas (7)-(9) and experimental results, respectively.

of resonators and the receiver with a two-port network, all the insight related to the resonator currents is lost, even though it dramatically simplifies the design process of the power electronic components and control system. The overall behaviour has been evaluated describing the system as a two-port network and a procedure to extract the parameters of the impedance matrix has been established; moreover, generalized analytical expressions of the impedance matrix terms have been proposed and validated both numerically and experimentally. Then, the parameters of an equivalent real transformer model have been extracted in order to establish a formal analogy between the resonator array and a traditional transformer. The results of the calculations carried out clearly indicate that, apart from the magnetizing reactance, the equivalent network chosen for the transformer presents parameters that are dramatically dependent on the receiver position, especially when the receiver is aligned with the last cells of the array. Despite the magnetizing reactance is constant for any receiver position, a not negligible magnetizing current is generally required and thus $\hat{Z}_m$ cannot be neglected.

The analytical and experimental results are in very good agreement, with a maximum error of about 10% for the parameter $\hat{Z}_{rr}$. Overall, these apparatuses allow the tolerance to the receiver misalignment to be dramatically increased, improving the coupling between the first array resonator and the receiver coil, at the expense of having circuit parameters dependent on the receiver position.

Conflict of interest

The authors declare no potential conflict of interests.

References

1. Bi S, Ho CK, Zhang R. Wireless powered communication: Opportunities and challenges. *IEEE Communications Magazine* 2015; 53(4): 117–125. doi: 10.1109/MCOM.2015.7081084

2. Yi Y, Buttner U, Fan Y, Foulds IG. Design and optimization of a 3-coil resonance-based wireless power transfer system for biomedical implants. *International Journal of Circuit Theory and Applications* 2015; 43(10): 1379-1390. doi: https://doi.org/10.1002/cta.2024

3. Smeets JP, Overboom TT, Jansen JW, Lomonova EA. Comparison of position-independent contactless energy transfer systems. *IEEE Transactions on Power Electronics* 2013; 28(4): 2059–2067. doi: 10.1109/TPEL.2012.2205404

4. Covic GA, Boys JT. Modern trends in inductive power transfer for transportation applications. *IEEE Journal of Emerging and Selected Topics in Power Electronics* 2013; 1(1): 28–41. doi: 10.1109/JESTPE.2013.2264473

5. Simonazzi M, Campanini A, Sandrolini L, Rossi C. Design Procedure Based on Maximum Efficiency for Wireless Power Transfer Battery Chargers with Lightweight Vehicle Assembly. *Energies* 2022; 15(1). doi: 10.3390/en15010070

6. Hui SYR, Zhong W, Lee CK. A Critical Review of Recent Progress in Mid-Range Wireless Power Transfer. *IEEE Transactions on Power Electronics* 2014; 29(9): 4500-4511. doi: 10.1109/TPEL.2013.2249670

7. Stevens CJ. Some consequences of the properties of metamaterials for wireless power transfer. In: 2015 9th International Congress on Advanced Electromagnetic Materials in Microwaves and Optics, METAMATERIALS 2015. ; Nov. 2015: 295–297

8. Lee J, Lee K, Cho DH. Stability Improvement of Transmission Efficiency Based on a Relay Resonator in a Wireless Power Transfer System. *IEEE Transactions on Power Electronics* 2017; 32(5): 3297-3300.

9. Miranda dCM, Pichorim SF, Abatti PJ. On the impact of relay circuit losses in four-coil wireless power transfer systems. *International Journal of Circuit Theory and Applications* 2019; 47(12): 1922-1932. doi: https://doi.org/10.1002/cta.2685

10. Kamalapathi K, Srinivasa Rao Nayak P, Kumar Tyagi V. Development and analysis of three-coil wireless charging system for electric vehicles. *International Journal of Circuit Theory and Applications* 2022; 50(1): 249-271. doi: https://doi.org/10.1002/cta.3158

11. Wang M, Wang H, Zhang Y, Shi Y, Yang L. Operating characteristics of four-coil magnetic resonant coupling wireless power transfer under different resonant states. *International Journal of Circuit Theory and Applications* 2021; 49(2): 415-429. doi: https://doi.org/10.1002/cta.2850

12. Stevens CJ. Magnetoinductive waves and wireless power transfer. *IEEE Transactions on Power Electronics* 2015; 30(11): 6182–6190. doi: 10.1109/TPEL.2014.2369811

13. Lee CK, Zhong WX, Hui SYR. Effects of Magnetic Coupling of Nonadjacent Resonators on Wireless Power Domino-Resonator Systems. *IEEE Transactions on Power Electronics* 2012; 27(4): 1905-1916. doi: 10.1109/TPEL.2011.2169460

14. Simonazzi M, Sandrolini L, Reggiani U. Magnetic Near Field Investigation and Shielding Effectiveness Evaluation of an Inductive Power Transfer System with a Resonator Array. In: 2020 International Symposium on Electromagnetic Compatibility - EMC EUROPE. ; 2020: 1-5.

15. Sandoval FS, Moazenzadeh A, Wallrabe U. Comprehensive Modeling of Magnetoinductive Wave Devices for Wireless Power Transfer. *IEEE Transactions on Power Electronics* 2018; 33(10): 8905-8915. doi: 10.1109/TPEL.2017.2779606

16. Sandoval FS, Moazenzadeh A, Delgado SMT, Wallrabe U. Double-spiral coils and live impedance modulation for efficient wireless power transfer via magnetoinductive waves. In: 2016 IEEE Wireless Power Transfer Conference (WPTC). ; 2016: 1-4

17. Lo YK, Lin JY, Yen SC, Lin LC. Analysis and design of a two-transformer active-clamping ZVS isolated inverse-SEPIC converter. *International Journal of Circuit Theory and Applications* 2014; 42(2): 111-126. doi: https://doi.org/10.1002/cta.1840

18. Lu R, Hossain MK, Alexander JI, Massoud Y, Haider MR. An efficient DC-DC converter for inductive power transfer in low-power sensor applications. *International Journal of Circuit Theory and Applications* 2022; 50(8): 2887-2899. doi: https://doi.org/10.1002/cta.3285

19. Rehlaender P, Schafmeister F, Bocker J, Grote T. Analytical Topology Comparison for a Single Stage On-Board EV-Battery Converter. In: . 2019-June. IEEE International Symposium on Industrial Electronics. ; 2019: 2477–2482

20. Esteban B, Sid-Ahmed M, Kar NC. A Comparative Study of Power Supply Architectures in Wireless EV Charging Systems. *IEEE Transactions on Power Electronics* 2015; 30(11): 6408-6422. doi: 10.1109/TPEL.2015.2440256

21. Lin BR, Nian YB. Soft-switching converter with low circulating current and wide range of ZVS turn-on. *International Journal of Circuit Theory and Applications* 2016; 44(2): 328-341. doi: https://doi.org/10.1002/cta.2077

22. Costanzo A, Dionigi M, Mastri F, Mongiardo M, Russer JA, Russer P. Rigorous design of magnetic-resonant wireless power transfer links realized with two coils. In: European Microwave Week 2014: Connecting the Future, EuMW 2014 - Conference Proceedings; EuMC 2014: 44th European Microwave Conference. ; 2014: 414–417

23. Costanzo A, Dionigi M, Mastri F, Mongiardo M, Russer JA, Russer P. Rigorous network modeling of magnetic-resonant wireless power transfer. *Wireless Power Transfer* 2014; 1(1): 27–34.

24. Brizi D, Fontana N, Barmada S, Monorchio A. An Accurate Equivalent Circuit Model of Metasurface-Based Wireless Power Transfer Systems. In: . 1. IEEE Open Journal of Antennas and Propagation. ; 2020: 549-559

25. Simonazzi M, Reggiani U, Sandrolini L. Standing Wave Pattern and Distribution of Currents in Resonator Arrays for Wireless Power Transfer. *Energies* 2022; 15(2). doi: 10.3390/en15020652

26. Simonazzi M, Sandrolini L, Mariscotti A. Receiver-Coil Location Detection in a Dynamic Wireless Power Transfer System for Electric Vehicle Charging. *Sensors* 2022; 22(6). doi: 10.3390/s22062317

27. Sandrolini L, Reggiani U, Puccetti G, Neau Y. Equivalent circuit characterization of resonant magnetic coupling for wireless transmission of electrical energy. *International Journal of Circuit Theory and Applications* 2013; 41(7): 753-771. doi: https://doi.org/10.1002/cta.1873

28. Simonazzi M, Sandrolini L, Zarri L, Reggiani U, Alberto J. Model of Misalignment Tolerant Inductive Power Transfer System for EV Charging. In: 2020 IEEE 29th International Symposium on Industrial Electronics (ISIE). ; 2020; Delft, The Netherlands, June 17-19: 1617-1622

29. Alberto J, Reggiani U, Sandrolini L. Circuit model of a resonator array for a WPT system by means of a continued fraction. In: 2016 IEEE 2nd International Forum on Research and Technologies for Society and Industry Leveraging a Better Tomorrow, RTSI 2016. ; 2016.

30. Alberto J, Reggiani U, Sandrolini L, Albuquerque H. Fast calculation and analysis of the equivalent impedance of a wireless power transfer system using an array of magnetically coupled resonators. *Progress In Electromagnetics Research B* 2018; 80: 101–112.

AUTHOR BIOGRAPHY

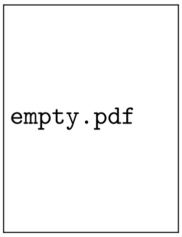

Author Name. This is sample author biography text this is sample author biography text.